IEEE Photonics Journal
An IEEE Photonics Society Publication

Open Access

The Particle Induced Mode Splitting and Exceptional Points in Whispering-Gallery Mode Microcavity

Volume 12, Number 6, December 2020

Jin Xiao-Xue
Yong-Pan Gao
Zheng Shi-Hui
Tie-Jun Wang
Chuan Wang

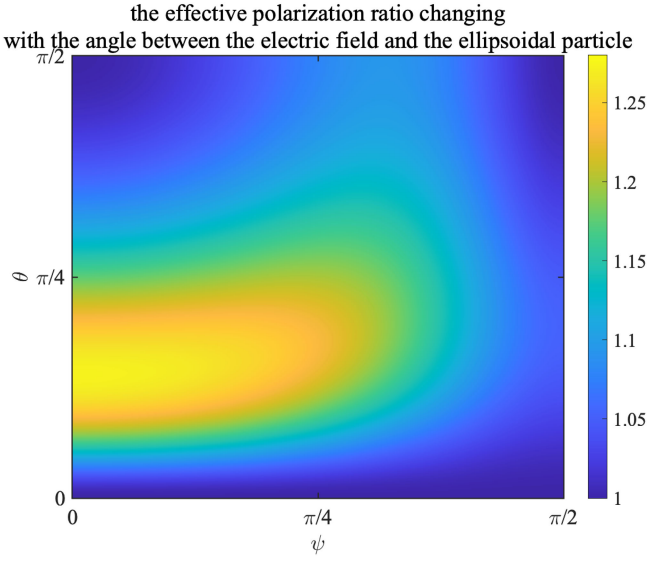

DOI: 10.1109/JPHOT.2020.3030702

The Particle Induced Mode Splitting and Exceptional Points in Whispering-Gallery Mode Microcavity

Jin Xiao-Xue,[1,2,3] **Yong-Pan Gao,**[1,2,3] **Zheng Shi-Hui,**[1,2,3] **Tie-Jun Wang,**[1,2,3] **and Chuan Wang**[1,2,3]

[1]School of Science and the State Key Laboratory of Information Photonics and Optical Communications, Beijing University of Posts and Telecommunications, Beijing 100876, China
[2]School of Cyberspace Security, Beijing University of Posts and Telecommunications, Beijing 100876, China
[3]School of Artificial Intelligence, Beijing Normal University, Beijing 100875, China

DOI:10.1109/JPHOT.2020.3030702

Manuscript received August 2, 2020; revised October 5, 2020; accepted October 8, 2020. Date of publication October 21, 2020; date of current version October 29, 2020. This work was supported in part by the Ministry of Science and Technology of the People's Republic of China (MOST) under Grant 2016YFA0301304 and in part by the National Natural Science Foundation of China through Grants 61671083 and 61622103; the Fundamental Research Funds for the Central Universities (BNU).
Corresponding author: Yong-Pan Gao. (e-mail: 768829204@qq.com).

Abstract: The manipulation of optical modes is an important issue for the realization of sensors in microcavities. In this paper, the generation and modulation of mode splitting in optical microcavities is studied by controlling the axes of an ellipsoidal nanoparticle. Different from the previous schemes, mode splitting and mode broadening caused by ellipsoidal particle scattering are related to the axial orientation of the particle. Therefore, unlike the scheme in which the relative position of the bi-spherical particles must be adjusted to modulate the relative coupling phase, the coupling strength and dissipation of the mode could be tuned by controlling the axial orientation of the ellipsoidal particle in our scheme. Furthermore, it can also tune the system to the exceptional points. This provides a novel way to manipulate the exceptional points in the whispering-gallery mode microcavity.

Index Terms: Whispering gallery mode, exceptional point, mode splitting.

1. Introduction

Whispering gallery mode(WGM) microcavity has become a research hotspot [1]–[3] for its very high quality factor and small mode volume, which could greatly enhance the interaction between light and matter [4]–[7]. Therefore, it has been extensively studied both theoretically and experimentally in these related fields [8]–[11], such as optical information processing [12], [13], microwave photonics [14]–[16], quantum computing [17]–[19], cavity quantum electrodynamics [20]–[25], and nonlinear optics [26]–[29].Furthermore, WGM optical microcavities are also widely used in the low threshold lasers [2], [30], parametric oscillators [31]–[34], high-precision sensing [4], [35]–[40] and so on.

In all of these applications, the WGM sensing [41]–[43] is one of the most fascinating topics. As far as we know, the optical WGM resonator can be used for force sensing [44]–[46], electric and magnetic fields detection [47]–[49], gas sensing [50]–[54], temperature sensing [55]–[57],

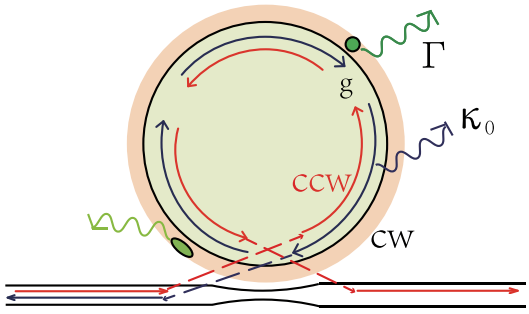

Fig. 1. The model consists of a spherical nanoparticle and an ellipsoidal nanoparticle coupled with the evanescent field of the WGM microcavity. The light field is coupled into the microsphere cavity through the fiber taper, g represents the coupling coefficient and Γ represents the damping rate. CW and CCW are the degenerate clockwise and counterclockwise modes of the WGM microcavity.

ultrasonic [58]–[60] and nanoparticle sensing [42], [61], [62], etc. The method of sensing using WGM microcavities can be divided into three categories: the mode splitting [63]–[66], the mode broadening [61], [67]–[70] and frequency shift [68]. Recently, exceptional points (EPs) sensing schemes have been given out which bring us a completely different idea from previous sensing solutions, and bring unprecedented sensing sensitivity [42], [71].

EPs sensing can be implemented by adjusting the relative position of two spherical nanoparticles to work in a unidirectional state of WGM, and this state is extremely sensitive to environmental changes, so ultra-sensitive sensing can be achieved. [71]. In addition to spherical particles, ellipsoidal nanoparticle will also scatter the electric field and bring new scattering characteristics. Recently, the theory has been proved that the axial orientation of ellipsoidal nanoparticle scattering has different effects on the coupling coefficients of different modes in the WGM cavity [72]. This undoubtedly provides a new implementation and physical mechanism to achieve mode modulation and EPs in the WGM cavity.

In this paper, we study the mode modulation and EPs of a WGM cavity, which is coupled with single spherical and elliptical nanoparticles through the evanescent field. The effective coupling coefficients of the clockwise(CW) and counterclockwise(CCW) modes can be controlled separately by rotating the ellipsoidal particle [72]. This inconsistency in coupling strength naturally breaks the symmetry of the modes in CW and CCW directions, so we can use this characteristic to modulate the system mode and achieve system EPs. It is worth noting that this implementation method does not need to modulate the relative phase, which means that we don't need to modulate the relative position of the particles, but only to adjust the axial orientation of the ellipsoidal particle. The method undoubtedly provides a new method for mode modulation and EPs sensing in the WGM microcavity.

2. The Theoretical Model

Here in our scheme, the model consists of a spherical microcavity evanescently coupled with a spherical nanoparticle and an ellipsoidal nanoparticle. As shown in Fig. 1, there are two WGM modes in the microcavity, namely the clockwise (CW) and counterclockwise (CCW) modes. These two modes are coupled by the scattering of spherical and ellipsoidal particles. Then, the total Hamiltonian of our scheme can be expressed as:

$$H = H_0 + H_1 + H_2, \tag{1a}$$

$$H_0 = \sum_p \hbar\omega_c a_p^\dagger a_p + \sum_j \hbar\omega_j b_j^\dagger b_j, \tag{1b}$$

$$H_1 = \sum_{n=0,1} \sum_{p,p'} \hbar g_{n,p,p'} a_p^\dagger a_{p'}, \tag{1c}$$

$$H_2 = \sum_{n=0,1} \hbar g_{n,j,p} (b_j^\dagger a_p + a_p^\dagger b_j), \tag{1d}$$

The total Hamiltonian can be divided into three parts: H_0 is the free Hamiltonian of the WGM and its reservoir environment, H_1 corresponds to the scattering induced coupling between the WGMs, the Hamiltonian H_2 represents the scattering induced coupling between the two nanoparticles and the surrounding reservoir. ω_c indicates the eigenfrequency of the microcavity and ω_j represents the eigenfrequency of the j-th reservoir mode, $a_p^\dagger$ and a_p represent the creation operator and annihilation operator of the cavity mode with $p(p')$ respectively denoting the CW(CCW) mode. $b_j(b_j^\dagger)$ is the j-th reservoir mode. $g_{n,p,p'}$ is the coupling coefficient generated by the n-th nanoparticle, $g_{n,j,p}$ shows the coupling between the scatterers and the reservoir.

A. The TE Mode

Since the spherical particle and the ellipsoidal particle are both sub-wavelength particles and located in different positions of the WGM microcavity. The relative phase factor $e^{\pm i\phi_n}$ must be considered. Due to the different orientation of the ellipsoidal particle, the induced coupling strength and dissipation are different for different modes. The effective polarizabilities of the coupling polarization and dissipative polarization for the transverse electric (TE) mode [72] are $\alpha_{n,g} = [\overleftrightarrow{\alpha} \cdot \mathbf{n}(\xi)]^\dagger \cdot \mathbf{n}(\xi)$ and $|\alpha_{n,\Gamma}| = |\overleftrightarrow{\alpha} \cdot \mathbf{n}(\xi)|$, where $\mathbf{n}(\xi)$ represents the unit vector of the polar position ξ. Then the coupling coefficients can be expressed as

$$g_0 = -\frac{\alpha_{0,g} f^2(\mathbf{r}) \omega_c}{2V_c}, \tag{2a}$$

$$\Gamma_0 = -\frac{f^2(\mathbf{r})}{V_c} |\alpha_{0,\Gamma}|^2 \frac{\omega_c^4}{6\pi v^3}, \tag{2b}$$

$$g_1 = -\frac{\alpha_{1,g} f^2(\mathbf{r}) \omega_c}{2V_c}, \tag{2c}$$

$$\Gamma_1 = -\frac{f^2(\mathbf{r})}{V_c} |\alpha_{1,\Gamma}|^2 \frac{\omega_c^4}{6\pi v^3}. \tag{2d}$$

where $f(\mathbf{r})$ is the cavity mode function at the scatter position $\mathbf{r}$, V_c is the mode volumn and v represents the speed of light in the surrounding environment. The Heisenberg equation of motion of the system can be described as

$$\begin{aligned} \frac{da_{cw(ccw)}}{dt} = &-i \left[\omega_c + \sum_{n=0,1} \left(g_n - \frac{i}{2} \right) \Gamma_n - \frac{i(\kappa_0 + \kappa_1)}{2} \right] a_{cw(ccw)} \\ &-i \left[\sum_{n=0,1} (g_n - \Gamma_n) e^{\pm 2i\phi_n} \right] a_{ccw(cw)} - \sqrt{\kappa_1} a_{cw(ccw)}^{in}. \end{aligned} \tag{3}$$

where κ_0 is the intrinsic damping rate of the cavity mode and κ_1 is the coupling rate to the taper. Then we set $a'_{cw(ccw)} = a_{cw(ccw)}e^{i\omega t}$, so Eq. 3 can be expressed as:

$$\begin{aligned} 0 = -\Bigg[-i\Delta_c + \sum_{n=0,1}\left(ig_n + \frac{1}{2}\Gamma_n\right) + \frac{\kappa_0+\kappa_1}{2}\Bigg] a_{cw(ccw)} \\ - \sum_{n=0,1}\left(ig_n + \frac{1}{2}\Gamma_n\right)\frac{1}{2}e^{\pm 2i\phi_n}) - \sqrt{\kappa_1}a^{in}_{cw(ccw)}. \end{aligned} \tag{4}$$

According to $(a^{in}_{cw}, a^{out}_{ccw}) = (1, 0)$, the expression of the transmission is

$$\begin{aligned} t &= 1 - \sqrt{\kappa_1}a_{cw} \\ &= 1 - \frac{\kappa_1 K}{K^2 - (\sum_{n=0,1} h_n)(\sum_{n=0,1} h_n^*)}, \end{aligned} \tag{5a}$$

$$K = -i\Delta_c + \sum_{n=0,1}(ig_n + \frac{1}{2}\Gamma_n) + \kappa, \tag{5b}$$

$$h_n = (ig_n + \frac{1}{2}\Gamma_n)e^{2i\phi_n}, \tag{5c}$$

$$\kappa = \frac{\kappa_0 + \kappa_1}{2}. \tag{5d}$$

B. The TM Mode

Considering the anisotropy of the ellipsoidal particle and the polarization of the electric field, the transverse magnetic(TM) mode has opposite direction of the electric field for the CW and the CCW modes. The effective polarizabilities of the coupling polarization and dissipative polarization can be written as: $\alpha^{p,p'}_{1,g} = [\overleftrightarrow{\alpha}\cdot\mathbf{n}_p(\xi)]^\dagger \cdot \mathbf{n}_{p'}(\xi)$ and $|\alpha^{p}_{1,\Gamma}| = |\overleftrightarrow{\alpha}\cdot\mathbf{n}_p(\xi)|$, where $p(p')$ represents the CW mode (CCW mode). The coupling coefficient and the damping rate of the ellipsoidal scatterer can be written as:

$$g_{1,p,p'} = -\frac{\alpha^{p,p'}_{1,g} f^2(\mathbf{r})\omega_c}{2V_c}, \tag{6a}$$

$$\Gamma_{1,p} = -\frac{f^2(\mathbf{r})}{V_c}|\alpha^{p}_{1,\Gamma}|\frac{\omega_c^4}{6\pi v^3}. \tag{6b}$$

Then, the Heisenberg equation of motion of the TM mode is:

$$\begin{aligned} \frac{\mathrm{d}a_{cw(ccw)}}{\mathrm{d}t} = -i\Bigg[\omega_c + \sum_{n=0,1}\left(g_{n,cw(ccw),cw(ccw)} - \frac{i}{2}\Gamma_{n,cw(ccw)}\right) \\ - \frac{i(\kappa_0+\kappa_1)}{2}\Bigg]a_{cw(ccw)} - i\Bigg[\sum_{n=0,1}\Bigg(g_{n,cw(ccw),ccw(cw)} \\ - \frac{i}{2}\Gamma_{n,ccw(cw)}\Bigg)e^{\pm 2i\phi_n}\Bigg]a_{ccw(cw)} - \sqrt{\kappa_1}a^{in}_{cw(ccw)}. \end{aligned} \tag{7}$$

According to the input-output relationship, the transmission spectrum of the system can be described as:

$$t = 1 - \sqrt{\kappa_1}a_{cw} = 1 - \frac{\kappa_1 D}{AD - BC}, \tag{8}$$

Here the coefficients A, B, C and D could be expressed as

$$A = -i\Delta_c + \sum_{n=0,1}\left(ig_{n,cwcw} + \frac{1}{2}\Gamma_{n,cw}\right) + \frac{\kappa_0+\kappa_1}{2}, \tag{9a}$$

$$B = \sum_{n=0,1}\left(ig_{n,cwccw} + \frac{1}{2}\Gamma_{n,ccw}\right)e^{2i\phi_n} \tag{9b}$$

$$C = \sum_{n=0,1}\left(ig_{n,ccwcw} + \frac{1}{2}\Gamma_{n,cw}\right)e^{-2i\phi_n} \tag{9c}$$

$$D = -i\Delta_c + \sum_{n=0,1}\left(ig_{n,ccwccw} + \frac{1}{2}\Gamma_{n,ccw}\right) + \frac{\kappa_0+\kappa_1}{2} \tag{9d}$$

From the above equations, we can conclude that the transmission spectrum can be adjusted by tuning the orientation of the ellipsoidal particle.

3. The Effective Tuning of the Mode Broadening and Mode Splitting Using Electric Field Vectors

As mentioned above, the relationship between polarization tensor and polarization rate is $\alpha_{n,g} = [\overleftrightarrow{\alpha}\cdot\mathbf{n}(\xi)]^{\dagger}\cdot\mathbf{n}(\xi)$ and $|\alpha_{n,\Gamma}| = |\overleftrightarrow{\alpha}\cdot\mathbf{n}(\xi)|$. The polarizability of the ellipsoidal particle $\overleftrightarrow{\alpha}$ and the electric field direction $\mathbf{n}(\xi)$ is

$$\overleftrightarrow{\alpha} = \begin{pmatrix}\alpha_x & 0 & 0\\ 0 & \alpha_y & 0\\ 0 & 0 & \alpha_z\end{pmatrix}, \quad \mathbf{n}(\xi) = \begin{pmatrix}n_x\\ n_y\\ n_z\end{pmatrix} \tag{10}$$

For an ellipsoid particle with the semi-major axes (x, y, z), we have

$$\begin{aligned}\alpha_i &= 4\pi xyz\frac{\varepsilon_1-\varepsilon_m}{3\varepsilon_m + 3L_i(\varepsilon_1-\varepsilon_m)},\\ L_i &= \frac{xyz}{2}\int_0^{\infty}\frac{dq}{(i^2+q)f(q)}, \qquad i = x, y, z.\\ f(q) &= \sqrt{(q+x^2)(q+y^2)(q+z^2)},\end{aligned} \tag{11}$$

The coupling strength and dissipation of TE and TM modes both can be adjusted by the angle of the particle. For simplicity, we take the TE mode as an example in the following discussion. And we also take the rotating frame with the cavity frequency. Then, the coupling function between the CW and CCW modes can be written as:

$$\frac{\mathrm{d}}{\mathrm{d}t}\begin{bmatrix}a_{cw}\\ a_{ccw}\end{bmatrix} = \begin{bmatrix}-\sum_{n=0,1}(ig_n+\frac{1}{2}\Gamma_n) & -\sum_{n=0,1}(ig_n+\frac{1}{2}\Gamma_n)e^{2i\phi_n}\\ -\sum_{n=0,1}(ig_n+\frac{1}{2}\Gamma_n)e^{-2i\phi_n} & -\sum_{n=0,1}(ig_n+\frac{1}{2}\Gamma_n)\end{bmatrix}\begin{bmatrix}a_{cw}\\ a_{ccw}\end{bmatrix}. \tag{12}$$

From the coupling equation matrix, the total frequency shift and the total linewidth broadening after adding the two scatterers is: $g_{total} = \sum_{n=0,1} g_n$ and $\Gamma_{total} = \sum_{n=0,1}\Gamma_n$. Here we define

$$g_{total} = -\frac{\alpha_{eff1}f^2(r)\omega_c}{2V_c}, \tag{13a}$$

$$\Gamma_{total} = -\frac{f^2(r)}{V_c}|\alpha^p_{eff2}|\frac{\omega_c^4}{6\pi v^3}, \tag{13b}$$

Here we set these two nanoparticles have the same $f(\mathbf{r})$ which is the mode distribution at the position $\mathbf{r}$ on the surface of WGM microcavity. Then, we have

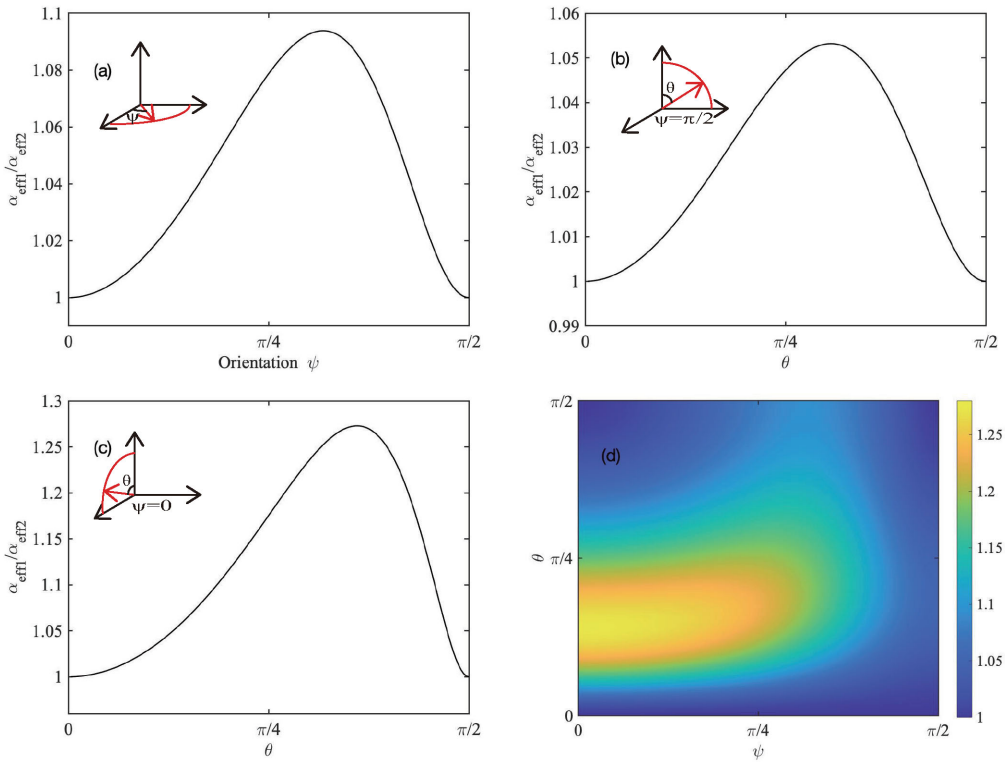

Fig. 2. Changing the angle between the electric field and the ellipsoidal particle, the effective polarization ratio between frequency splitting and linewidth broadening changes accordingly. (a) The electric field is parallel to the equatorial plane and the angle between the electric field and the longest semimajor axis of the ellipsoidal particle varys from 0 to $\pi/2$. (b) $\psi = \pi/2$ and (c) $\psi = 0$, the angle between the electric field and the shortest semimajor axis changes from 0 to $\pi/2$. (d) The effective polarization ratio changes with θ and ψ varying from 0 to $\pi/2$.

$$\alpha_{eff1} = \alpha_x \cdot n_x^2 + \alpha_y \cdot n_y^2 + \alpha_z \cdot n_z^2 + \alpha_0, \tag{14a}$$

$$\alpha_{eff2} = \sqrt{(\alpha_x \cdot n_x)^2 + (\alpha_y \cdot n_y)^2 + (\alpha_z \cdot n_z)^2} + \alpha_0. \tag{14b}$$

Here, α_0 represents $x = y = z$ in Eq.11, which characterizes the contribution of spherical particle. In order to study the polarization characteristics of our model in detail, we assume that $(\alpha_x, \alpha_y, \alpha_z) = (3, 1, 1/3) * \alpha_0$. The ratio of the effective polarization $(\alpha_{eff1}/\alpha_{eff2})$ is shown in Fig. 2. First of all, we need to pay attention to the point when $\theta = 0$ and $\psi = 0$. The polarization ratio at these points is $\alpha_{eff1} = \alpha_{eff2}$. This is the same as the case of pure spherical particles, because one of the three axes of the ellipsoid is in the same orientation as the electric field, and only this axis can be polarized in this situation. Figs. 2(a), (b), and (c) show how the polarization ratio changes with the particle rotation on the *xoy*, *yoz*, and *zox* surfaces. We can find that when the electric field revolves in different plane, the system changes differently. Comparing the figure (a), (b) and (c), we find that the polarization changes with the direction of the particle more obviously in (c).This is because the axial lengths of different axes of ellipsoidal particle are different, and the polarizability of the system varies with the axis of the ellipsoidal particle.

The polarizability of the particle will change with the direction of the field. However, the polarization of the particle in this scheme is usually not directly measurable. But, the total coupling strength g_{total} and dissipation Γ_{total} are measurable. Based on Eq.13, we studied the case where g_{total} and Γ_{total} change with the orientation of particle when $(\alpha_x, \alpha_y, \alpha_z) = (3, 1, 1/3) * \alpha_0$. Figs. 3(a) and (b)

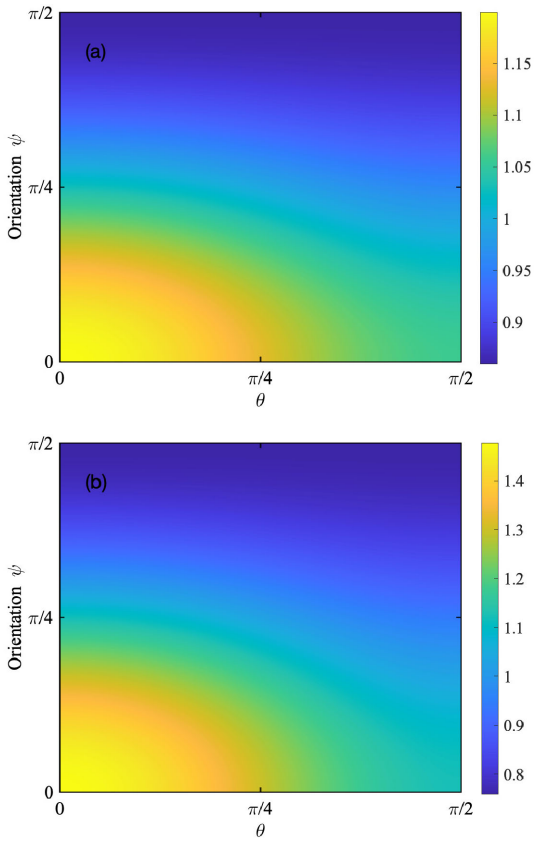

Fig. 3. Frequency splitting (a) and linewidth broadening (b) changed with the angle between the direction of the electric field and the ellipsoidal particle. The figure indicates the ratio of the frequency splitting or linewidth broadening generated by ellipsoidal and spherical particles to frequency splitting or linewidth broadening generated by two spherical particles. The radius of spherical particles are 150 nm, and semimajor axes of the ellipsoidal particle are 450 nm, 150 nm, and 50 nm.

show that the coupling strength and dissipation vary with the orientations ψ and θ, respectively. It shows that we can modulate the coupling strength and dissipation by changing the particle orientation. Furthermore, we find that the dissipation is more sensitive to the change of the particle orientation. It's due to that there is a quadratic relationship between the change in dissipation and the change in orientation angle.

Generally, the increase in spectral width will reduce the accuracy of our spectral measurement. When the mode splitting is smaller than the mode broadening, the splitting of transmission spectrum can not be measured, so the relationship between mode splitting and mode broadening needs to be considered. Fig. 4 shows the ratio of the mode splitting to the mode broadening varies with the two semi-major axes (L_x and L_y in unit of L_z) of the ellipsoidal particle, wherein one of the semimajor axis ($L_z = 50\,nm$) of the ellipsoidal particle remains constant. The orientation of the nanoparticle is $\theta = \psi = \pi/4$. When the polar axes of the ellipsoidal particle are close in the x and y directions($L_x \approx L_y$), the ratio is larger for smaller particle as the shape of the particle is approximately circular under this situation and the scattering field is relatively uniform. Compared to the condition when the particle is ellipsoidal, more light is scattered back into the cavity. Then, the dissipation will decrease and the ratio will increase. On the other hand, the spectral resolution can be increased by increasing the volume of the particle. So, the requirement for the consistency of $L_x - L_y$ semimajor axes of the particle will also be reduced. When the particle is larger, the direction

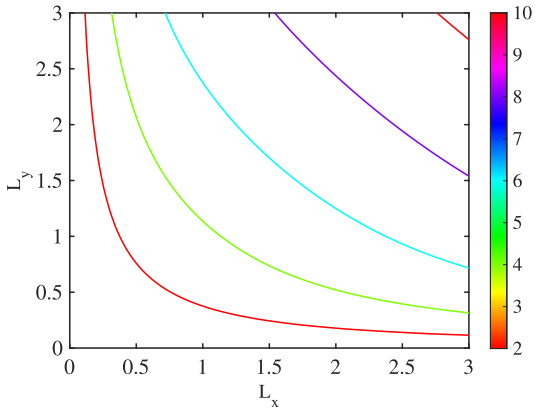

Fig. 4. The total ratio of mode splitting and mode broadening change with the change of two semi-major axes of the ellipsoidal particle while keeping the shortest semi-major axes (L_z) of the ellipsoidal particle constant.

of the scattered field will decrease, then the coupling strength and dissipation strength are only related to the volume and the orientation of the particle.

4. Transmission Spectra Under the Control of Ellipsoidal Nanoparticle Axis Angle

To study the degenerate characteristics or EPs of the system, we go back to Eq.12. Under the steady state, the complex eigenfrequency of the system is:

$$\omega_{\pm} = i(g_1 + g_2) + \frac{\Gamma_1 + \Gamma_2}{2} \pm \sqrt{\left(ig_1 + \frac{\Gamma_1}{2}\right)^2 + \left(ig_2 + \frac{\Gamma_2}{2}\right)^2 + 2\cos(2\phi_1)\left(ig_1 + \frac{\Gamma_1}{2}\right)\left(ig_2 + \frac{\Gamma_2}{2}\right)} \tag{15}$$

Firstly, when the $\theta = 0$, this is equivalent to placing two particles in the same position, then there will be no interface term. The mode of the WGM cavity must be the state of mode splitting under single particle scattering. Secondly, when the under square term is zero, the system will be degenerate $\Delta = \omega_+ - \omega_- = 0$. Then the same as previous EPs sensing scheme, we assume that there is a perturbation on the first particle δg. Then we have

$$\begin{aligned}\Delta &= 2\sqrt{\left(i(g_1 + \delta g + \frac{\Gamma_1}{2}\right)^2 + \left(ig_2 + \frac{\Gamma_2}{2}\right)^2 + 2\cos(2\phi_1)\left(ig_1 + \frac{\Gamma_1}{2}\right)\left(ig_2 + \frac{\Gamma_2}{2}\right)} \\ &\approx \sqrt{2\,(g - i\Gamma/2)\,\delta g} \gg \delta g\end{aligned} \tag{16}$$

As shown in Fig. 5, we have plotted the relationship between frequency shift and δg in a minimal interval, where the red curve represents EPs and the blue curve represents DPs. In this interval, the value of the frequency shift at EPs is always slightly larger than the value at DPs. The illustration shows the curve between the two dashed lines of 10–11 *MHz*. For the sake of comparison, we move the DPs up to make the value approximate to the value of EPs at 10 *MHz*.

So, EPs sensing is extremely sensitive. Then, we should show that we can get the EPs in our system. As mentioned above, the coupling strength can be modulated by the orientation of the particle. Compared to the case of an ellipsoidal particle, this orientation-dependent coupling modulation will also lead to the degeneracy of the cavity modes. In general, there are two ways to modulate the coupling of the system to make it degenerate : changing the angle between the two particles, and changing the angle between the ellipsoidal particle and the electric field. Here we

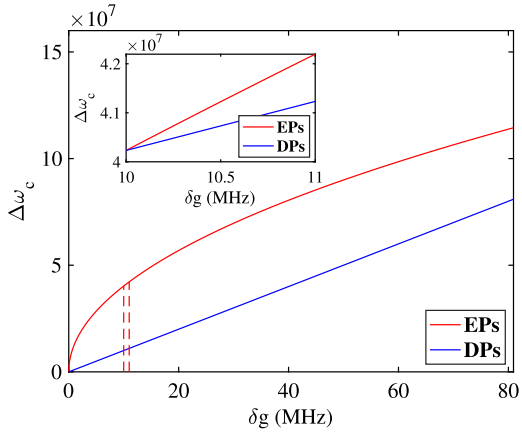

Fig. 5. Frequency shift changes with δg in a small interval. The red curve is EP and the blue curve is DP. The insert shows that the value range of δg is $10^7 - 1.1 * 10^7$ *Hz*. For the convenience of comparison, we shift DP up to make it the same as EP at 10^7 *Hz*. .

have studied the situation where the system works on the TE mode with the transmission coefficient shown in Eq.5.

Firstly, we tune the relative phase of these two particles. As shown in Fig. 6, we assume the orientation of the ellipsoidal particle is $\theta = \psi = \pi/3$. Here we set the radius of the spherical particle as 90 nm, and the ellipsoidal particle semimajor axes are 270 nm, 90 nm and 30 nm. The transmission spectrum as a function of the phase angle ϕ is numerically simulated in Fig. 6(a). We can find there is only one peak in the transmission spectrum when the coupling phase $\phi = \pi/2$. In order to see the changes in the eigen-frequency of the spectrum more clearly, we show the eigen-frequency as a function of the coupling phase in Fig. 6(b). It can be seen that when the phase is $\pi/2$, mode degeneracy occurs and the system works on the Exceptional Points(EPs) [42], [71] which can be used to enhance the sensitivity. Fig. 6(c) shows the full width at half maximum(FWHM) at the transmission spectrum as a function of the phase angle ϕ. We calculate the Q at the EPs of the microcavity, because the frequency and dissipation of the two modes at EPs are degenerate, so Q is also degenerate. It is well known that the frequency of 1550 nm laser is $1.92 * 10^{14}$ and the cavity loss is $\kappa = 3.71 * 10^6$, so the value of Q is $5.2 * 10^7$.

Compared to the previous studies, it is required to modulate the relative positions of the particles. Different from the solution in Fig. 6 for adjusting the relative positions of two particles, the solution in Fig. 7 is to adjust the orientation of the ellipsoidal particle. And we can see that adjusting the angle of the ellipsoidal particle has a different effect on the spectrum than adjusting the relative position of two particles. In our scheme, the introduction of the ellipsoidal particle providing a way to avoid this situation, we can adjust the orientation of the nanoparticle to modulate the transmission spectrum. By fixing the relative phase of the quantum particles as $\phi = \pi/2$, and assuming that the radius of the spherical particle is 150 nm, and the semimajor axes of ellipsoidal particle are 450 nm, 150 nm and 50 nm, we modulate both azimuths (θ and ψ) of the ellipsoidal particle at the same time as shown in Fig. 7(a). We can find the transmission spectrum is single peak when $\theta = \psi = 5\pi/24$. Fig. 7(b) shows that the eigen-frequency of the cavity modes change with orientation of ellipsoidal particle. It can be found that the system can also be tuned to the exceptional points. What's more, different from Fig. 6(b), only one mode will shift in this scheme, which will provide us a stable reference frequency. Fig. 7(c) shows the change in the FWHM at the peak of the transmission spectrum as orientation of ellipsoidal particle changes. Although the FWHM changes irregularly when the angle changes, it can be seen that the FWHM at EPs is equal.

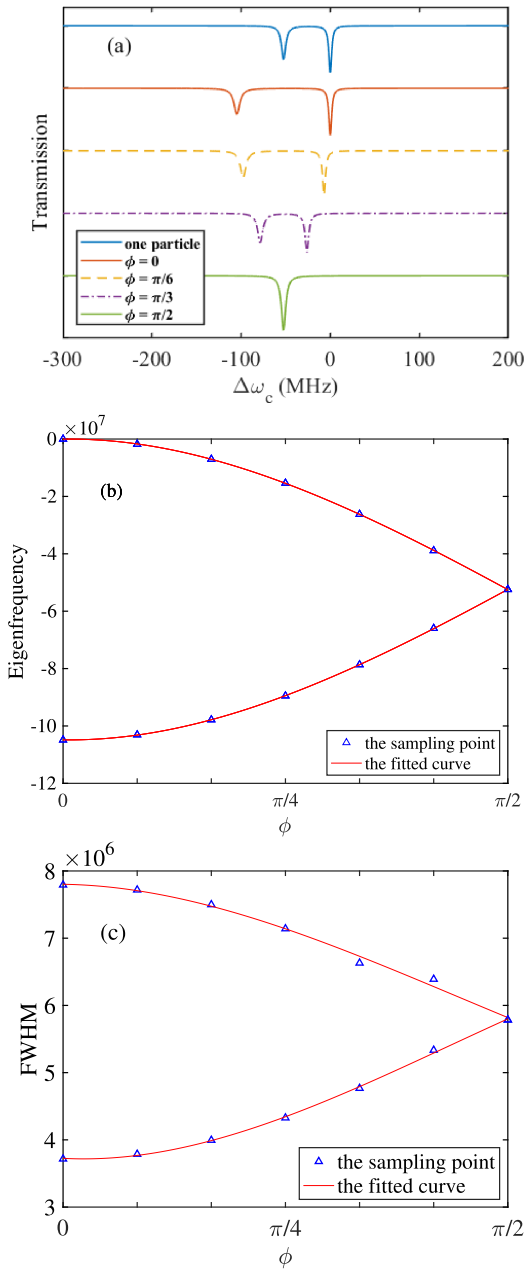

Fig. 6. (a) The transmission spectrum varies with the phase angle keeping the angle between the electric field and the ellipsoidal particle constant. The blue curve is the transmission spectrum curve when only one spherical nanoparticle is present in the evanescent field of the microcavity. The transmission spectrum changes after an ellipsoidal particle placed in the evanescent field, and the angles between the electric and the ellipsoidal particle are $\theta = \pi/3$, $\psi = \pi/3$ and the phase angle is 0. When the phase angle is $\pi/2$, the transmission spectrum appears degenerate. (b) Mode splitting varies as the phase angle changes from 0 to $\pi/2$. The triangle is the frequency of the peak value of the transmission spectrum generated by each phase change, and the red curve is a fitted curve according to the values obtained from the sampling points. (c) The full width at half maximum varies with the phase angle from 0 to $\pi/2$. The blue triangle is the full width at half maxima of the peak value of the transmission spectrum generated by each phase change, and the red curve is fitted by the sampling points. Assuming that the radius of the spherical particle is $r = 90$ nm, and the semimajor axes of the ellipsoidal particle are $r_x = 270$ nm, $r_y = 90$ nm, $r_z = 30$ nm. .

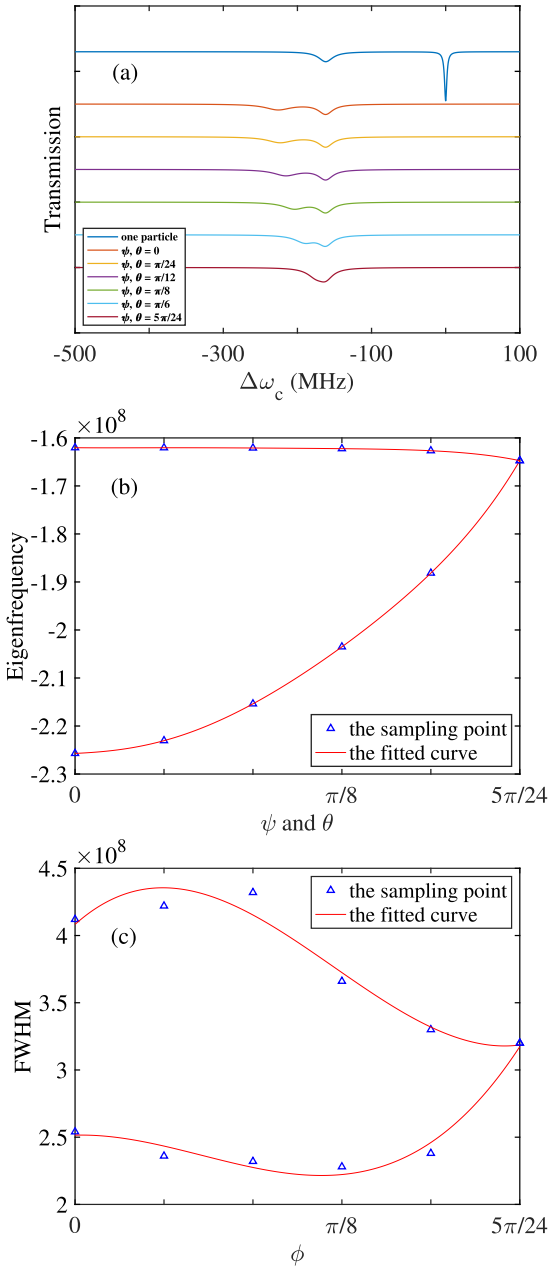

Fig. 7. (a) Keeping the phase angle unchanged, the transmission spectrum of the microcavity changes with the angle between the electric field and the ellipsoidal particle. The blue curve is the transmission spectrum in the presence of only one spherical particle. The transmission spectrum is changed after disposing an ellipsoidal particle, and the phase angle is $\pi/2$, and the orientation of the electric field is parallel to the maximum semi-major axis of the ellipsoidal particle. When θ and ψ are both $5\pi/24$, the transmission appears degenerate. (b) The frequency of the peak of the transmission varies with the angle corresponding to the sampling point in (a). The interval between the sampling points θ and ψ is $\pi/24$. The triangle is the frequency of the peak value obtained after changing the angle between the electric field direction and the ellipsoidal particle, and the red curve is fitted according to the triangle. (c) The full width at half maximum varies with the angle corresponding to the sampling point in (a). The triangle is the full width at half maximum of the peak of transmission spectrum in (a), and the red curve is fitted according to the triangle. It is assumed that the radius of spherical particle is 150 nm, and the semimajor axes of the ellipsoidal particle are 450 nm, 150 nm, and 50 nm.

5. Summary

In summary, we studied the properties of the optical modes in the WGM microcavity surrounded by an isotropic spherical scatter and an anisotropic ellipsoidal scatter. Taking advantage of the anisotropic particle scattering characteristics, we realize nanoparticle orientation tunable mode splitting and EPs. Based on this idea, firstly, we studied the ratio changes at different rates on different planes of the coordinates by comparing the effective coupling polarization with the dissipation polarization. Secondly, we studied the scattering properties of the system under different L_x and L_y, and found that when the consistency of L_x and L_y is stronger, the scattering spectrum is more distinguishable. Finally, when we studied the mode modulation and EPs generation, we find that we can modulate the mode of system by modulating the orientation of a particle. Lastly, we find we can make the system switch between EPs and normal mode splitting with this method. Our research enriches the implementation and mechanism of mode control and EPs in the WGM cavity.

References

[1] K. J. Vahala, "Optical microcavities," *Nature*, vol. 424, no. 6950, pp. 839–846, 2003. [Online]. Available: https://doi.org/10.1038/nature01939

[2] J. Ward and O. Benson, "Wgm microresonators: Sensing, lasing and fundamental optics with microspheres," *Laser & Photon. Rev.*, vol. 5, no. 4, pp. 553–570, 2011. [Online]. Available: https://onlinelibrary.wiley.com/doi/abs/10.1002/lpor.201000025

[3] H. Cao and J. Wiersig, "Dielectric microcavities: Model systems for wave chaos and non-hermitian physics," *Rev. Mod. Phys.*, vol. 87, pp. 61–111, Jan. 2015. [Online]. Available: https://link.aps.org/doi/10.1103/RevModPhys.87.61

[4] F. Vollmer and L. Yang, "Review label-free detection with high-q microcavities: A review of biosensing mechanisms for integrated devices," *Nanophotonics*, vol. 1, pp. 267–291, Dec. 2012. [Online]. Available: https://doi.org/10.1515/nanoph-2012-0021

[5] J. R. Lopez, E. Treasurer, K. M. Snyder, D. Keng, and S. Arnold, "Whispering gallery mode coulometry of the nanoparticle-microcavity interaction in aqueous solution," *Appl. Phy. Lett.*, vol. 112, p. 051109, Jan. 2018. [Online]. Available: https://doi.org/10.1063/1.5017041

[6] J. Xavier, S. Vincent, F. Meder, and F. Vollmer, "Advances in optoplasmonic sensors combining optical nano/microcavities and photonic crystals with plasmonic nanostructures and nanoparticles," *Nanophotonics*, vol. 7, no. 3–4, pp. 1–38, 2017. [Online]. Available: https://doi.org/10.1515/nanoph-2017-0064

[7] J. Su, A. F. Goldberg, and B. M. Stoltz, "Label-free detection of single nanoparticles and biological molecules using microtoroid optical resonators," *Light: Sci. & Appl.*, vol. 5, pp. e16 001–e16 001, 2016. [Online]. Available: https://doi.org/10.1038/lsa.2016.1

[8] K. D. Heylman *et al.*, "Optical microresonators as single-particle absorption spectrometers," *Nature Photon.*, vol. 10, p. 788795, 2016. [Online]. Available: https://doi.org/10.1038/nphoton.2016.217

[9] L. He, Ş. K. Özdemir, J. Zhu, W. Kim, and L. Yang, "Detecting single viruses and nanoparticles using whispering gallery microlasers," *Nature Nanotechnol.*, vol. 6, pp. 428–432, 2011. [Online]. Available: https://doi.org/10.1038/nnano.2011.99

[10] W. Yu, W. C. Jiang, Q. Lin, and T. Lu, "Cavity optomechanical spring sensing of single molecules," *Nature Commun.*, vol. 7, p. 12311, 2016. [Online]. Available: https://doi.org/10.1038/ncomms12311

[11] X.-W. Zhang, L.-Y. Liu, and L. Xu, "Ultralow sensing limit in optofluidic micro-bottle resonator biosensor by self-referenced differential-mode detection scheme," *Appl. Phy. Lett.*, vol. 104, p. 033703, 2014. [Online]. Available: https://doi.org/10.1063/1.4861596

[12] E. S. Sedov *et al.*, "Tunneling-assisted optical information storage with lattice polariton solitons in cavity-qed arrays," *Phys. Rev. A*, vol. 89, p. 033828, Mar. 2014. [Online]. Available: https://link.aps.org/doi/10.1103/PhysRevA.89.033828

[13] E. Jané, M. B. Plenio, and D. Jonathan, "Quantum-information processing in strongly detuned optical cavities," *Phys. Rev. A*, vol. 65, p. 050302, May 2002. [Online]. Available: https://link.aps.org/doi/10.1103/PhysRevA.65.050302

[14] M. Goryachev and M. E. Tobar, "Reconfigurable microwave photonic topological insulator," *Phys. Rev. Appl.*, vol. 6, p. 064006, Dec. 2016. [Online]. Available: https://link.aps.org/doi/10.1103/PhysRevApplied.6.064006

[15] P. V. Parimi, W. T. Lu, P. Vodo, J. Sokoloff, J. S. Derov, and S. Sridhar,"Negative refraction and left-handed electromagnetism in microwave photonic crystals," *Phys. Rev. Lett.*, vol. 92, p. 127401, Mar. 2004. [Online]. Available: https://link.aps.org/doi/10.1103/PhysRevLett.92.127401

[16] S. Bittner, B. Dietz, M. Miski-Oglu, and A. Richter, "Extremal transmission through a microwave photonic crystal and the observation of edge states in a rectangular dirac billiard," *Phys. Rev. B*, vol. 85, p. 064301, Feb. 2012. [Online]. Available: https://link.aps.org/doi/10.1103/PhysRevB.85.064301

[17] T. Pellizzari, S. A. Gardiner, J. I. Cirac, and P. Zoller, "Decoherence, continuous observation, and quantum computing: A cavity qed model," *Phys. Rev. Lett.*, vol. 75, pp. 3788–3791, Nov. 1995. [Online]. Available: https://link.aps.org/doi/10.1103/PhysRevLett.75.3788

[18] M. Feng, "Quantum computing with trapped ions in an optical cavity via raman transition," *Phys. Rev. A*, vol. 66, p. 054303, Nov. 2002. [Online]. Available: https://link.aps.org/doi/10.1103/PhysRevA.66.054303

[19] Q. Chen and M. Feng, "Quantum-information processing in decoherence-free subspace with low-*q* cavities," *Phys. Rev. A*, vol. 82, p. 052329, Nov. 2010. [Online]. Available: https://link.aps.org/doi/10.1103/PhysRevA.82.052329
[20] Y. P. Gao, C. Cong, T. J. Wang, Z. Yong, and C. Wang, "Cavity-mediated coupling of phonons and magnons," *Phys. Rev. A*, vol. 96, no. 2, 2017.
[21] B. C. Sanders, S. D. Bartlett, B. Tregenna, and P. L. Knight, "Quantum quincunx in cavity quantum electrodynamics," *Phys. Rev. A*, vol. 67, p. 042305, Apr. 2003. [Online]. Available: https://link.aps.org/doi/10.1103/PhysRevA.67.042305
[22] L. Childress, A. S. Sørensen, and M. D. Lukin, "Mesoscopic cavity quantum electrodynamics with quantum dots," *Phys. Rev. A*, vol. 69, p. 042302, Apr. 2004. [Online]. Available: https://link.aps.org/doi/10.1103/PhysRevA.69.042302
[23] Y.-P. Gao, X.-F. Liu, T.-J. Wang, C. Cao, and C. Wang, "Photon excitation and photon-blockade effects in optomagnonic microcavities," *Phys. Rev. A*, vol. 100, no. 4, p. 043831, 2019.
[24] A. J. Campillo, J. D. Eversole, and H.-B. Lin, "Cavity quantum electrodynamic enhancement of stimulated emission in microdroplets," *Phys. Rev. Lett.*, vol. 67, pp. 437–440, Jul. 1991. [Online]. Available: https://link.aps.org/doi/10.1103/PhysRevLett.67.437
[25] J. F. Triana and J. L. Sanz-Vicario, "Revealing the presence of potential crossings in diatomics induced by quantum cavity radiation," *Phys. Rev. Lett.*, vol. 122, p. 063603, Feb. 2019. [Online]. Available: https://link.aps.org/doi/10.1103/PhysRevLett.122.063603
[26] "The analysis of high-order sideband signals in optomechanical system," *Sci. China(Physics, Mech. & Astronomy)*, vol. v.61, no. 9, pp. 99–102, 2018.
[27] T. K. Allison, A. Cingöz, D. C. Yost, and J. Ye, "Extreme nonlinear optics in a femtosecond enhancement cavity," *Phys. Rev. Lett.*, vol. 107, p. 183903, Oct. 2011. [Online]. Available: https://link.aps.org/doi/10.1103/PhysRevLett.107.183903
[28] V. S. Ilchenko, A. A. Savchenkov, A. B. Matsko, and L. Maleki, "Nonlinear optics and crystalline whispering gallery mode cavities," *Phys. Rev. Lett.*, vol. 92, p. 043903, Jan. 2004. [Online]. Available: https://link.aps.org/doi/10.1103/PhysRevLett.92.043903
[29] A. S. Rogov and E. E. Narimanov, "Nonlinear optics at low powers: Alternative mechanism of on-chip optical frequency comb generation," *Phys. Rev. A*, vol. 94, p. 063832, Dec. 2016. [Online]. Available: https://link.aps.org/doi/10.1103/PhysRevA.94.063832
[30] V. Sandoghdar, F. Treussart, J. Hare, V. Lefèvre-Seguin, J. M. Raimond, and S. Haroche, "Very low threshold whispering-gallery-mode microsphere laser," *Phys. Rev. A*, vol. 54, pp. R1777–R1780, Sep. 1996. [Online]. Available: https://link.aps.org/doi/10.1103/PhysRevA.54.R1777
[31] D. M. Whittaker, "Effects of polariton-energy renormalization in the microcavity optical parametric oscillator," *Phys. Rev. B*, vol. 71, p. 115301, Mar. 2005. [Online]. Available: https://link.aps.org/doi/10.1103/PhysRevB.71.115301
[32] A. Baas, J.-P. Karr, M. Romanelli, A. Bramati, and E. Giacobino, "Optical bistability in semiconductor microcavities in the nondegenerate parametric oscillation regime: Analogy with the optical parametric oscillator," *Phys. Rev. B*, vol. 70, p. 161307, Oct. 2004. [Online]. Available: https://link.aps.org/doi/10.1103/PhysRevB.70.161307
[33] T. J. Kippenberg, S. M. Spillane, and K. J. Vahala, "Kerr-nonlinearity optical parametric oscillation in an ultrahigh-*q* toroid microcavity," *Phys. Rev. Lett.*, vol. 93, p. 083904, Aug. 2004. [Online]. Available: https://link.aps.org/doi/10.1103/PhysRevLett.93.083904
[34] J. J. Baumberg *et al.*, "Parametric oscillation in a vertical microcavity: A polariton condensate or micro-optical parametric oscillation," *Phys. Rev. B*, vol. 62, pp. R16 247–R16 250, Dec. 2000. [Online]. Available: https://link.aps.org/doi/10.1103/PhysRevB.62.R16247
[35] G. Yong-Pan, W. Tie-Jun, C. Cong, and W. Chuan, "Gap induced mode evolution under the asymmetric structure in a plasmonic resonator system," *Photon. Res.*, vol. 5, no. 2, pp. 113–, 2017.
[36] F. Vollmer and S. Arnold, "Whispering-gallery-mode biosensing: label-free detection down to single molecules," *Nature Methods*, vol. 5, pp. 591–596, 2008. [Online]. Available: https://doi.org/10.1038/nmeth.1221
[37] C. You *et al.*, "Identification of light sources using machine learning," *Appl. Phy. Rev.*, vol. 7, no. 2, p. 021404, 2020.
[38] Y.-P. Gao *et al.*, "Effective mass sensing using optomechanically induced transparency in microresonator system," *IEEE Photon. J.*, vol. 9, no. 1, Feb. 2016, Art. no. 6800411.
[39] M. R. Foreman, J. D. Swaim, and F. Vollmer, "Whispering gallery mode sensors," *Adv. Opt. Photon.*, vol. 7, pp. 168–240, 2015. [Online]. Available: https://aop.osa.org/abstract.cfm?URI=aop-7-2-168
[40] Y. Zhi, X.-C. Yu, Q. Gong, L. Yang, and Y.-F. Xiao, "Single nanoparticle detection using optical microcavities," *Adv. Mater.*, vol. 29, p. 1604920, 2017. [Online]. Available: https://doi.org/10.1002/adma.201604920
[41] B.-Q. Shen *et al.*, "Detection of single nanoparticles using the dissipative interaction in a high-*q* microcavity," *Phys. Rev. Appl.*, vol. 5, p. 024011, Feb. 2016. [Online]. Available: https://link.aps.org/doi/10.1103/PhysRevApplied.5.024011
[42] J. Wiersig, "Enhancing the sensitivity of frequency and energy splitting detection by using exceptional points: Application to microcavity sensors for single-particle detection," *Phys. Rev. Lett.*, vol. 112, p. 203901, May 2014. [Online]. Available: https://link.aps.org/doi/10.1103/PhysRevLett.112.203901
[43] Y.-L. Chen and Y.-Z. Huang, "Multinanoparticle scattering in a multimode microspheroid resonator," *Phys. Rev. A*, vol. 99, p. 023818, Feb. 2019. [Online]. Available: https://link.aps.org/doi/10.1103/PhysRevA.99.023818
[44] T. Ioppolo, M. Kozhevnikov, V. Stepaniuk, M. V. Ötügen, and V. Sheverev, "Micro-optical force sensor concept based on whispering gallery mode resonators," *Appl. Opt.*, vol. 47, no. 16, pp. 3009–3014, Jun. 2008. [Online]. Available: https://ao.osa.org/abstract.cfm?URI=ao-47-16-3009
[45] T. Ioppolo, U. K. Ayaz, and M. V. Ötügen, "High-resolution force sensor based on morphology dependent optical resonances of polymeric spheres," *J. Appl. Phy.*, vol. 105, pp. 013 535–013 535, 2009. [Online]. Available: https://doi.org/10.1063/1.3054338
[46] A. Motazedifard, A. Dalafi, F. Bemani, and M. H. Naderi, "Force sensing in hybrid bose-einstein-condensate optomechanics based on parametric amplification," *Phys. Rev. A*, vol. 100, p. 023815, Aug. 2019. [Online]. Available: https://link.aps.org/doi/10.1103/PhysRevA.100.023815
[47] A. Ali, T. Ioppolo, and M. V. Ötügen, "Beam-coupled microsphere resonators for high-resolution electric field sensing," *Proc. SPIE - The Int. Soc. Opt. Eng.*, vol. 8600, Mar. 2013.

[48] D.-N. Peligrad *et al.*, "Cavity perturbation by superconducting films in microwave magnetic and electric fields," *Phys. Rev. B*, vol. 58, pp. 11 652–11 671, Nov. 1998. [Online]. Available: https://link.aps.org/doi/10.1103/PhysRevB.58.11652
[49] T. A. Fisher *et al.*, "Electric-field and temperature tuning of exciton-photon coupling in quantum microcavity structures," *Phys. Rev. B*, vol. 51, pp. 2600–2603, Jan. 1995. [Online]. Available: https://link.aps.org/doi/10.1103/PhysRevB.51.2600
[50] M. Gregor, C. Pyrlik, R. Henze, A. Wicht, A. Peters, and O. Benson, "An alignment-free fiber-coupled microsphere resonator for gas sensing applications," *Appl. Physics Lett.*, vol. 96, pp. 231 102–231 102, 2010. [Online]. Available: https://doi.org/10.1063/1.3430058
[51] Y. Sun, S. I. Shopova, G. Frye-Mason, and X. Fan, "Rapid chemical-vapor sensing using optofluidic ring resonators," *Opt. Lett.*, vol. 33, pp. 788–790, Apr. 2008. [Online]. Available: https://ol.osa.org/abstract.cfm?URI=ol-33-8-788
[52] N. Lin, L. Jiang, S. Wang, Q. Chen, H. Xiao, Y. Lu, and H. Tsai, "Simulation and optimization of polymer-coated microsphere resonators in chemical vapor sensing," *Appl. Opt.*, vol. 50, no. 28, pp. 5465–5472, Oct. 2011. [Online]. Available: https://ao.osa.org/abstract.cfm?URI=ao-50-28-5465
[53] N. A. Yebo, P. Lommens, Z. Hens, and R. Baets, "An integrated optic ethanol vapor sensor based on a silicon-on-insulator microring resonator coated with a porous zno film," *Opt. Express*, vol. 18, no. 11, pp. 11 859–11 866, May 2010. [Online]. Available: https://www.opticsexpress.org/abstract.cfm?URI=oe-18-11-11859
[54] B. Petrak, N. Djeu, and A. Muller, "Purcell-enhanced raman scattering from atmospheric gases in a high-finesse microcavity," *Phys. Rev. A*, vol. 89, p. 023811, Feb. 2014. [Online]. Available: https://link.aps.org/doi/10.1103/PhysRevA.89.023811
[55] B.-B. Li *et al.*, "On chip high-sensitivity thermal sensor based on high-*q* polydimethylsiloxane-coated microresonator," *Appl. Physics Lett.*, vol. 96, p. 251109, 2010. [Online]. Available: https://doi.org/10.1063/1.3457444
[56] R. Morino *et al.*, "Mode-selective thermal radiation from a microsphere as a probe of optical properties of high-temperature materials," *Phys. Rev. A*, vol. 95, p. 063814, Jun. 2017. [Online]. Available: https://link.aps.org/doi/10.1103/PhysRevA.95.063814
[57] L. L. Martín, C. Pérez-Rodríguez, P. Haro-González, and I. R. Martín, "Whispering gallery modes in a glass microsphere as a function of temperature," *Opt. Express*, vol. 19, no. 25, pp. 25 792–25 798, Dec. 2011. [Online]. Available: https://www.opticsexpress.org/abstract.cfm?URI=oe-19-25-25792
[58] M. V. Chistiakova and A. M. Armani, "Photoelastic ultrasound detection using ultra-high-q silica optical resonators," *Opt. Express*, vol. 22, pp. 28 169–28 179, Nov. 2014. [Online]. Available: https://www.opticsexpress.org/abstract.cfm?URI=oe-22-23-28169
[59] J. Pan, B. Zhang, Z. Liu, J. Zhao, Y. Feng, L. Wan, and Z. Li, "Microbubble resonators combined with a digital optical frequency comb for high-precision air-coupled ultrasound detectors," *Photon. Res.*, vol. 8, no. 3, pp. 303–310, Mar. 2020. [Online]. Available: https://www.osapublishing.org/prj/abstract.cfm?URI=prj-8-3-303
[60] L. Riobó, Y. Hazan, F. Veiras, M. Garea, P. Sorichetti, and A. Rosenthal, "Noise reduction in resonator-based ultrasound sensors by using a cw laser and phase detection," *Opt. Lett.*, vol. 44, no. 11, pp. 2677–2680, Jun. 2019. [Online]. Available: https://ol.osa.org/abstract.cfm?URI=ol-44-11-2677
[61] M. D. Baaske, M. R. Foreman, and F. Vollmer, "Single-molecule nucleic acid interactions monitored on a label-free microcavity biosensor platform," *Nature Nanotechnol.*, vol. 9, pp. 933–939, Aug. 2014. [Online]. Available: https://doi.org/10.1038/nnano.2014.180
[62] S. Li *et al.*, "Angular position detection of single nanoparticles on rolled-up optical microcavities with lifted degeneracy," *Phys. Rev. A*, vol. 88, p. 033833, Sep 2013. [Online]. Available: https://link.aps.org/doi/10.1103/PhysRevA.88.033833
[63] A. Mazzei, S. Götzinger, L. de S. Menezes, G. Zumofen, O. Benson, and V. Sandoghdar, "Controlled coupling of counterpropagating whispering-gallery modes by a single rayleigh scatterer: A classical problem in a quantum optical light," *Phys. Rev. Lett.*, vol. 99, p. 173603, Oct. 2007. [Online]. Available: https://link.aps.org/doi/10.1103/PhysRevLett.99.173603
[64] Ş. K. Özdemir *et al.* "Highly sensitive detection of nanoparticles with a self-referenced and self-heterodyned whispering-gallery raman microlaser," *Proc. Nat. Academy Sci.*, vol. 111, no. 37, pp. E3836–E3844, Sep. 2014. [Online]. Available: https://www.pnas.org/content/111/37/E3836
[65] J. Zhu, Ş. K. Özdemir, L. He, and L. Yang, "Controlled manipulation of mode splitting in an optical microcavity by two rayleigh scatterers," *Opt. Express*, vol. 18, no. 23, pp. 23 535–23 543, Nov. 2010. [Online]. Available: https://www.opticsexpress.org/abstract.cfm?URI=oe-18-23-23535
[66] J. Zhu, Ş. K. Özdemir, Y.-F. Xiao, L. Li, L. He, D.-R. Chen, and L. Yang, "On-chip single nanoparticle detection and sizing by mode splitting in an ultrahigh-*q* microresonator," *Nature Photon.*, vol. 4, pp. 46–49, 2010. [Online]. Available: https://doi.org/10.1038/nphoton.2009.237
[67] F. Vollmer, D. Braun, A. Libchaber, M. Khoshsima, I. Teraoka, and S. Arnold, "Protein detection by optical shift of a resonant microcavity," *Appl. Phys. Lett.*, vol. 80, p. 4057, 2002. [Online]. Available: https://doi.org/10.1063/1.1482797
[68] M. D. Baaske and F. Vollmer, "Optical observation of single atomic ions interacting with plasmonic nanorods in aqueous solution," *Nature Photon.*, vol. 10, pp. 733–739, 2016. [Online]. Available: https://doi.org/10.1038/nphoton.2016.177
[69] Y. Hu, L. Shao, S. Arnold, Y.-C. Liu, C.-Y. Ma, and Y.-F. Xiao, "Mode broadening induced by nanoparticles in an optical whispering-gallery microcavity," *Phys. Rev. A*, vol. 90, p. 043847, Oct. 2014. [Online]. Available: https://link.aps.org/doi/10.1103/PhysRevA.90.043847
[70] L. Shao *et al.*, "Detection of single nanoparticles and lentiviruses using microcavity resonance broadening," *Adv. Mater.*, vol. 25, pp. 5616–5620, Oct. 2013. [Online]. Available: https://doi.org/10.1002/adma201302572
[71] W. Chen, Ş. K. Özdemir, G. Zhao, J. Wiersig, and L. Yang, "Exceptional points enhance sensing in an optical microcavity," *Nature*, vol. 548, no. 7666, pp. 192–196, 2017. [Online]. Available: https://doi.org/10.1038/nature23281
[72] Y. Xu *et al.*, "Mode splitting induced by an arbitrarily shaped rayleigh scatterer in a whispering-gallery microcavity," *Phys. Rev. A*, vol. 97, p. 063828, Jun. 2018. [Online]. Available: https://link.aps.org/doi/10.1103/PhysRevA.97.063828